Structure
Article

Structural and Biophysical Studies of the Human IL-7/IL-7Rα Complex

Craig A. McElroy,[1] Julie A. Dohm,[2] and Scott T.R. Walsh[1,3,*]
[1]Department of Molecular and Cellular Biochemistry, College of Medicine, Comprehensive Cancer Center, Ohio State University, 467 Hamilton Hall, 1645 Neil Avenue, Columbus, OH 43210, USA
[2]University of Pennsylvania Law School, 3400 Chestnut Street, Philadelphia, PA 19104, USA
[3]Present address: Center for Advanced Research in Biotechnology, University of Maryland Biotechnology Institute, 9600 Gudelsky Drive, Rockville, MD 20850, USA
*Correspondence: walshs@umbi.umd.edu
DOI 10.1016/j.str.2008.10.019

SUMMARY

IL-7 and IL-7Rα bind the γ_c receptor, forming a complex crucial to several signaling cascades leading to the development and homeostasis of T and B cells. We report that the IL-7Rα ectodomain uses glycosylation to modulate its binding constants to IL-7, unlike the other receptors in the γ_c family. IL-7 binds glycosylated IL-7Rα 300-fold more tightly than unglycosylated IL-7Rα, and the enhanced affinity is attributed primarily to an accelerated on rate. Structural comparison of IL-7 in complex to both forms of IL-7Rα reveals that glycosylation does not participate directly in the binding interface. The SCID mutations of IL-7Rα locate outside the binding interface with IL-7, suggesting that the expressed mutations cause protein folding defects in IL-7Rα. The IL-7/IL-7Rα structures provide a window into the molecular recognition events of the IL-7 signaling cascade and provide sites to target for designing new therapeutics to treat IL-7-related diseases.

INTRODUCTION

IL-7, IL-7Rα, and γ_c form a ternary complex that plays fundamental roles in extracellular matrix remodeling, development, and homeostasis of T and B cells (reviewed in Mazzucchelli and Durum, 2007). IL-7Rα also crossreacts to form a ternary complex with thymic stromal lymphopoietin (TSLP) and its receptor (TSLPR), and activates the TSLP pathway, resulting in T and dendritic cell proliferation in humans and further B cell development in mice (Leonard, 2002). Tight regulation of the signaling cascades activated by the complexes is therefore crucial to normal cellular function. Understimulation of the IL-7 pathway caused by mutations in the IL-7Rα ectodomain inhibits T and B cell development, resulting in patients with a form of severe combined immunodeficiency (SCID) (Giliani et al., 2005; Puel et al., 1998). Overstimulation of the pathways leads to allergic rhinitis, autoimmunity, heart disease, and proliferation of cancers (reviewed in Sportes and Gress, 2007). In clinical trials of patients with hepatitis and recovering cancer patients, IL-7 is being tested to spark T cell development and expansion (reviewed in Sportes and Gress, 2007).

IL-7 and IL-7Rα belong to the γ_c family of cytokine receptors, which includes IL-2, -4, -9, -15, -21, and receptors. The ILs and ectodomains of the receptors share <15% sequence identity with each other including the binding interfaces (see Figure S1 available online). Besides binding γ_c, all of the ILs and receptors in the γ_c family are glycoproteins. Despite the universal glycosylation of the γ_c family, glycosylation has not been vital to the binding interactions among family members. Studies show that glycosylation plays no role in complex formation between IL-2 (Rickert et al., 2004), -4 (Hage et al., 1999), -15 (Matsumoto et al., 2003), -21 (Zhang et al., 2003), and receptors. Three Asns of IL-7 and six Asns of the IL-7Rα ectodomain may be N-linked glycosylated from the Asn-X-Ser/Thr recognition motif. Glycosylation of IL-7 does not affect its binding/function to IL-7Rα (Goodwin et al., 1989). It remains an open question to the importance of glycosylation of the IL-7Rα in binding and function.

To our knowledge for the first time among γ_c family members, we report that glycosylation is important to the interaction between IL-7 and IL-7Rα. We compare the binding constants of IL-7 to unglycosylated and glycosylated IL-7Rα and show that the enhanced binding affinity of IL-7 to glycosylated IL-7Rα results primarily from an accelerated on rate. Furthermore, we have determined the crystal structures of IL-7 complexes bound to unglycosylated IL-7Rα at 2.7 Å and glycosylated IL-7Rα at 2.9 Å. Glycosylation of IL-7Rα does not induce large conformational changes in the complexes and the glycans are located outside the IL-7/IL-7Rα binding interface, indicating an indirect mechanism of binding enhancement. The IL-7/IL-7Rα binding interface displays the smallest, least polar, and least specific interface in comparison to other IL/receptor complexes in the γ_c family. We map the mutations found in patients with SCID onto the IL-7Rα structure and show that they are localized outside the binding interface. Lastly, we discuss the possible mechanism of glycosylation of IL-7Rα with its binding interaction with IL-7.

RESULTS

IL-7/IL-7Rα Biosensor Analysis

The binding kinetics and affinities observed for the interactions between IL-7 and unglycosylated or glycosylated IL-7Rα reveal the importance of glycosylation in formation of the IL-7/IL-7Rα complex. Surface plasmon resonance (SPR) binding kinetics

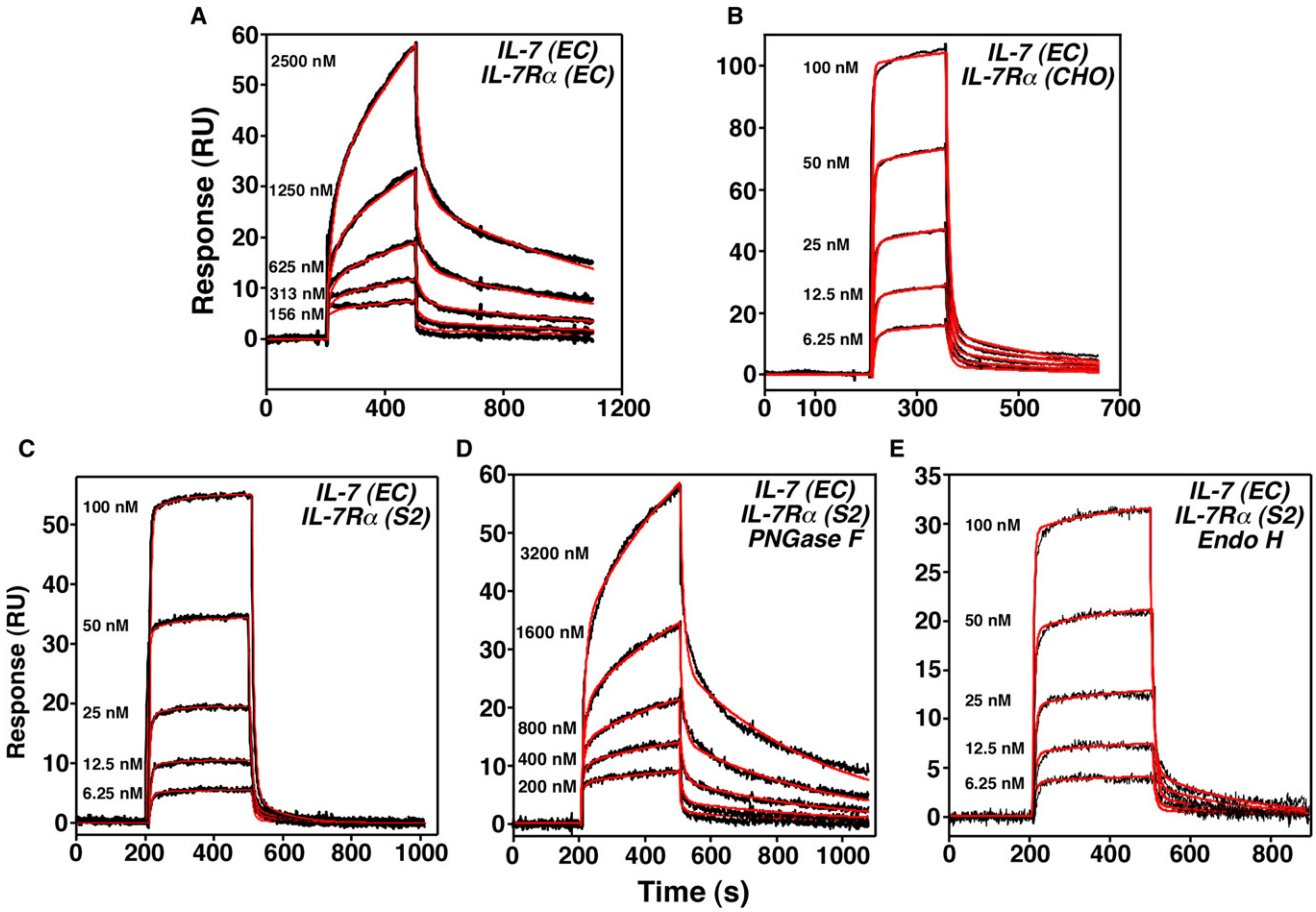

Figure 1. Binding Kinetic Sensorgrams for the IL-7/IL-7Rα Interaction Determined Using SPR

(A) Binding kinetics between unglycosylated IL-7 and IL-7Rα, both from *E. coli* (EC).

(B and C) Binding kinetics of IL-7 (EC) to glycosylated IL-7Rα from Chinese hamster ovary (CHO) and Schneider (S2) insect cells, respectively.

(D) Binding kinetics of IL-7 to PNGase F-treated IL-7Rα (S2).

(E) Binding kinetics between IL-7 (EC) and Endo H-treated IL-7Rα (S2).

The binding kinetics sensorgrams are in black. The red curves are global fits of the SPR data to a two-step binding reaction model to determine the binding kinetics.

collected on IL-7 from *Escherichia coli* (EC) and unglycosylated IL-7Rα (EC), glycosylated IL-7Rα from Chinese hamster ovary (CHO) cells, and glycosylated IL-7Rα from Schneider insect (S2) cells display biphasic kinetics that fit best to a two-state reaction mechanism with two on- and off-rate constants (Figure 1; Table 1). IL-7 binds to glycosylated IL-7Rα (CHO/S2) with k_1 rates that are 7100-fold (CHO) and 5200-fold (S2) faster than the k_1 rate of IL-7 binding to unglycosylated IL-7Rα (EC). The k_2 rates of IL-7 binding to the IL-7Rα glycoforms (CHO/S2) display negligible effects in the comparison of IL-7 binding to unglycosylated IL-7Rα (4.9-fold for CHO to EC and 1.7-fold for S2 to EC). Similarly, the two off rates, k_{-1} and k_{-2}, also show negligible effects in the comparison of IL-7 binding to glycosylated IL-7Rαs (CHO/S2) and unglycosylated IL-7Rα (7.1- and 2.4-fold for CHO to EC, and 5.9- and 3.4-fold for S2 to EC). Thus, the ~300-fold enhancement in K_d of IL-7 and glycosylated IL-7Rα (CHO/S2) relative to IL-7 and unglycosylated IL-7Rα (EC) derives primarily from an accelerated k_1 rate.

The enhanced k_1 and K_d of IL-7 to glycosylated IL-7Rα relative to unglycosylated IL-7Rα arises directly from N-glycosylation, but is insensitive to glycan composition. Binding studies of IL-7 with IL-7Rα (S2) treated with peptide:N-glycosidase F (PNGase F)—an enzyme that removes N-glycans and converts the Asns to Asps—resemble those performed on IL-7 and unglycosylated IL-7Rα (EC), indicating that the differences in binding result from N-glycosylation and not some attribute of using different cell expression systems (Figure 1D). The binding constants were also measured for IL-7 binding to glycosylated IL-7Rα expressed in two cell lines (CHO and S2) that modify proteins with different N-glycosylation patterns (Figures 1B and 1C). Unlike CHO cells, S2 cells do not incorporate complex branches with sialic acids or galactoses onto proteins, but express proteins with paucimannose hybrid glycans (Aoki et al., 2007). Even though the glycosylation patterns on IL-7Rα from S2 cells differ from those on IL-7Rα from CHO cells, the binding constants were comparable.

Binding is likely unaffected by the variations in glycan branching because the proximal N-acetylglucosamine (GlcNAc) is wholly responsible for the large enhanced k_1 on rate and affinity of IL-7 to glycosylated IL-7Rα. The binding constants measured for

Table 1. Binding Constants of IL-7 to IL-7Rα Variants

	k_1 ($M^{-1}s^{-1}$)	k_{-1} (s^{-1})	k_2 (s^{-1})	k_{-2} (s^{-1})	K_d[a]	IC_{50}[b]
wt-IL-7 (EC)						
IL-7Rα (EC)	2.1×10^2	1.7×10^{-2}	4.2×10^{-3}	1.2×10^{-3}	18 μM	3.0 μM
IL-7Rα (CHO)	1.5×10^6	1.2×10^{-1}	8.6×10^{-4}	2.9×10^{-3}	62 nM	ND
IL-7Rα (S2)	1.1×10^6	1.0×10^{-1}	2.5×10^{-3}	4.1×10^{-3}	56 nM	190 nM
IL-7Rα (S2 Endo H)	1.1×10^6	1.1×10^{-1}	1.4×10^{-3}	6.2×10^{-3}	82 nM	340 nM
IL-7Rα (S2 PNGase F)	2.4×10^3	8.3×10^{-2}	3.5×10^{-3}	2.3×10^{-3}	14 μM	2.2 μM
E106A-IL-7 (EC)						
IL-7Rα (S2)	1.9×10^5	1.7×10^{-2}	3.2×10^{-3}	1.0×10^{-3}	21 nM	ND
IL-7Rα (S2 PNGase F)	6.9×10^3	6.9×10^{-2}	6.0×10^{-3}	9.8×10^{-4}	1.4 μM	ND

ND, not determined. Surface plasmon resonance experiments were performed in 10 mM HEPES (pH 7.4), 150 mM NaCl, 3 mM EDTA, 0.005% Tween 20 at 25°C. Experiments were triplicated with standard errors < 10% for the rate constants.

[a] $K_d = k_{-1}k_{-2}/k_1(k_2 + k_{-2})$.

[b] Competition ELISA experiments were performed in PBS buffer (pH 7.4) with 0.05% Tween 20 at 25°C.

IL-7 to glycosylated IL-7Rα (S2) treated with endoglycosidase H (Endo H)—an enzyme that cleaves the bond between the first two GlcNAcs of hybrid mannose glycans like that produced from S2 cells, leaving the proximal GlcNAc—were similar to those measured for IL-7 to the fully glycosylated IL-7Rα (CHO/S2) (Figures 1B, 1C, and 1E). The SPR experiments measuring the affinities between IL-7 and unglycosylated IL-7Rα (EC) and glycosylated IL-7Rα (S2) untreated and treated with PNGase F or Endo H were further confirmed by competition ELISA experiments (Figure S2; Table 1).

IL-7/IL-7Rα Crystal Structure Determinations

We determined the crystal structures of IL-7 (EC, E106A mutation) bound to both unglycosylated and glycosylated forms of the IL-7Rα at 2.7 and 2.9 Å resolution, respectively. Similar binding constants were observed between the interactions of E106A-IL-7 with both forms of IL-7Rα compared to wt-IL-7 (Table 1). The unglycosylated complex was refined with a crystallographic R value (R_{cryst}) of 0.212 (R_{free} of 0.266; Table S1). Two unglycosylated IL-7/IL-7Rα (EC) complexes were located within the asymmetric unit. The glycosylated complex was refined to R_{cryst} and R_{free} values of 0.234 and 0.267, respectively (Table S2). One glycosylated IL-7 (EC)/IL-7Rα (S2) complex was located within the asymmetric unit.

IL-7 Structures

IL-7 adopts an up-up-down-down four-helix bundle topology with two crossover loops (Figure 2A). The α helices A–D vary in length from 13 to 22 residues, similar to the lengths of helices in other γ_c ILs. A turn of a π helix from T12–M17 in helix A is unique to IL-7 and stabilizes the IL-7/IL-7Rα interaction. The first crossover loop of 23 residues contains 1.5 turns of α helix (mini-helix 1), whereas the majority of the second crossover loop of 33 residues could not be traced in any of the three complex structures. The first crossover loop in IL-7 is positioned differently between the IL-7/IL-7Rα complex structures, probably from local crystal packing contacts.

The crystal structures of IL-7 clearly showed electron density to trace two out of three disulfide bonds (Figure 2A). The disulfide bonds are C34-C129, C47-C141, and C2-C92. This disulfide bond patterning is in contrast to homology models of IL-7 and biochemical data that predicted different locations by swapping the C47-C141 and C2-C92 disulfide bonds for C2-C141 and C92-C141 (Cosenza et al., 1997, 2000). Whereas the electron density allowed tracing of the C34-C129 and C47-C141 disulfide bonds, it was too weak near the N terminus (residues 1–6[7]) and the end of helix C proceeding into the second crossover loop (residues 89–123) to trace the third disulfide bond between C2 and C92. Similarly, electron density was absent for the N-terminal disulfide bond of a structure of IL-10 (Yoon et al., 2006).

Previous studies indicated that W142 of helix D, the sole Trp of IL-7, was critical to the interaction between IL-7 and γ_c (Cosenza et al., 2000; vanderSpek et al., 2002). However, the IL-7 structures show the burial of W142 into the hydrophobic core of the four-helix bundle, with the Nε forming a hydrogen bond (H bond) to T86 Oγ1 (Figure 2B). Thus, mutation of W142 likely causes defective folding of helix D and/or complete unfolding of IL-7, resulting in the reported decreases in cell assays (Cosenza et al., 2000; vanderSpek et al., 2002).

IL-7Rα Structures

IL-7Rα forms a L-shaped architecture similar to other IL receptors in the γ_c family, as well as other related receptors in the cytokine receptor class I (CRH I) superfamily, including receptors for growth hormone, erythropoietin, and other ILs (Figure 2C). The 219 residue IL-7Rα ectodomain folds into two fibronectin type III (FNIII) domains connected by a 3_{10}-helical linker. The elbow angle (ε) between the FNIII domains was similar in both IL-7Rα structures, ranging from 74° to 75° (Table S3). In the D1 domain of IL-7Rα, a disulfide bond ($C22_R$-$C37_R$) conserved among CRH I family members bridges β strands A1 and B1. Two other disulfide bonds unique to IL-7Rα connect β strands C1 to C′1 ($C54_R$-$C62_R$) and F1 to G1 ($C88_R$-$C98_R$). Another defining feature of the CRH I family found in IL-7Rα is the WSXWS sequence motif in the D2 domain. In IL-7Rα, the WSXWS motif forms extensive π cation side-chain stacking interactions critical to the SCID mutations discussed below.

IL-7Rα contains six potential N-glycosylation sites: $N29_R$, $N45_R$, $N131_R$, $N162_R$, $N212_R$, and $N213_R$. The electron density of glycosylated IL-7Rα allowed tracing of two GlcNAcs for three different Asns: $N29_R$, $N45_R$, and $N131_R$ (Figures 2C–2E). The side chain of $N162_R$ was clear in the electron density, but not its

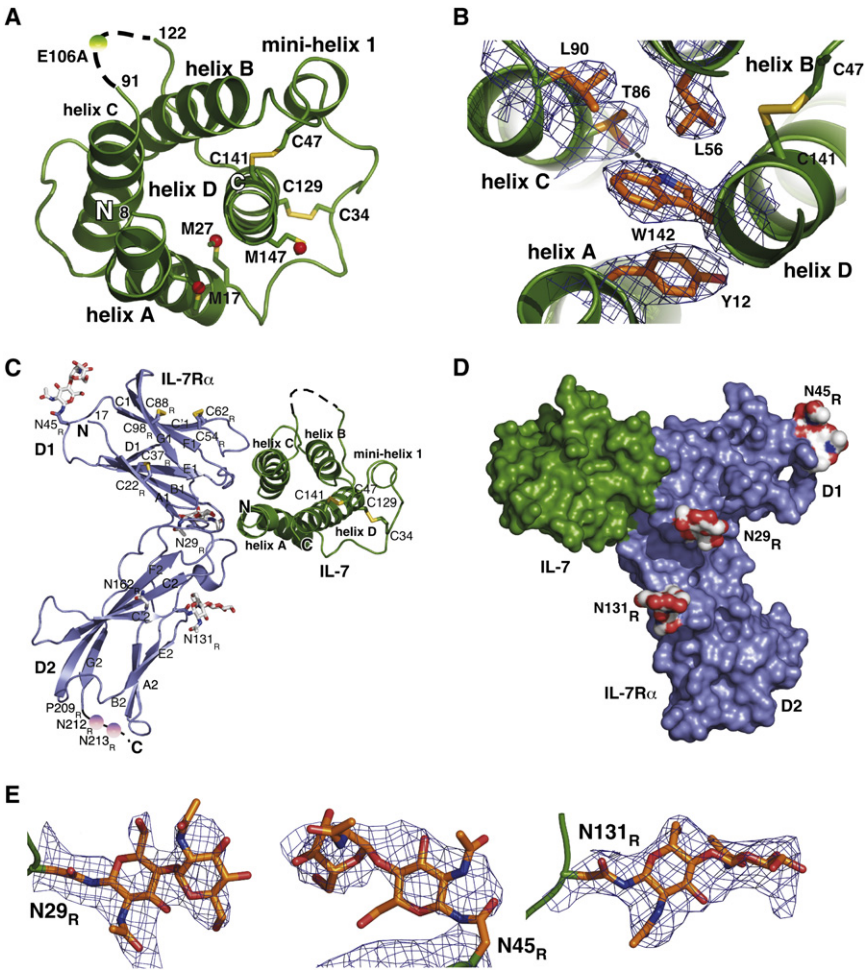

Figure 2. Structural Characterization of IL-7 with Unglycosylated and Glycosylated Forms of IL-7Rα

(A) One of the unglycosylated IL-7 structures oriented by placement of methionine residues into the experimentally determined SeMet heavy atoms (red spheres). Unobservable electron density in the second crossover loop is shown as a black dashed line. The E106A mutation in IL-7, which was used for both the unglycosylated and glycosylated complex structures, is highlighted as a green sphere.

(B) Close-up view of the hydrophobic core around the sole Trp residue of IL-7, W142. The σ_A-weighted $2F_o - F_c$ electron density map (blue mesh) contoured at 1.0σ. W142 Nε1 forms an H bond to T86 Oγ1 (black dashed line).

(C) Ribbon diagram of the glycosylated IL-7 (EC, green)/IL-7Rα (S2, purple) complex. Disulfide bonds are shown in yellow. IL-7Rα residues are labeled with a subscript R. The observed IL-7Rα GlcNAcs are shown as white sticks.

(D) Molecular surface of the glycosylated IL-7/IL-7Rα complex colored as in (C).

(E) Simulated annealed σ_A-weighted omit electron density maps (blue mesh) contoured at 1.0σ for the modeled GlcNAcs attached to $N29_R$, $N45_R$, and $N131_R$.

potential glycan. Because electron density was absent for residues $E210_R$-$D219_R$, neither $N212_R$ nor $N213_R$ could be traced. All of the Asn side chains modeled in the glycosylated structure were also observable in the unglycosylated structures, except residue $N29_R$, indicating extensive side-chain mobility. All of the glycans of the IL-7Rα structure are extending away from IL-7Rα, and none of the glycans are contacting other residues on IL-7Rα except the second GlcNAc (NAG 903) attached to $N45_R$, whose O6 glycan group is H bonding to $A48_R$ N (3.2 Å).

Comparison of IL-7 Bound to Unglycosylated and Glycosylated IL-7Rα

Although the overall structures of IL-7 bound to both forms of IL-7Rα are similar, a change in the position of the predicted γ_c binding interface suggests that glycosylation may also modulate the binding of γ_c to IL-7/IL-7Rα (Figure 3A). The two unglycosylated complexes superimpose with a root-mean-square deviation (rmsd) of 0.29 Å (164 Cα) for all secondary (2°) structural elements. Superimposing the 2° structural elements of the glycosylated structure onto either unglycosylated complex yield rmsds of 0.53 and 0.64 Å (159 Cα), demonstrating that the glycans do not induce large conformational changes. Independently, the IL-7 four-helix bundles superimpose with an rmsd of 0.52 Å (72 Cα, glycosylated structure to both unglycosylated structures), and the two IL-7Rα FNIII domains superimpose with an rmsd of 0.37 Å (86 Cα, glycosylated structure to both unglycosylated structures).

The surface on IL-7 where γ_c is predicted to bind (helices A and D) experienced the largest structural change between the unglycosylated and glycosylated structures (Figure 3A). When the complex structures are aligned on the IL-7Rαs using both D1 and D2 domains, the IL-7 four-helix bundles shift relative to one another with a displacement of individual helices ranging from 1° (helix B) to 5° (helix D) (Figure 3A). If the complex structures are aligned on the IL-7 four-helix bundles, then the D2 domains of the α receptors rotate accordingly. Similar displacements are observed between the glycosylated complex with both unglycosylated complexes, potentially ruling out changes induced by crystal contact formation. Thus, glycosylation of IL-7Rα may be positioning the four-helix bundle of IL-7 and/or the domains of the IL-7Rα in a manner conducive for γ_c binding. Further studies will probe whether glycosylation of IL-7Rα modulates the binding constants, structure, and function of γ_c.

IL-7/IL-7Rα Interface

IL-7 is positioned at the elbow region connecting the D1 and D2 domains of IL-7Rα (Figures 2C, 2D, and 3A). The interface largely comprises hydrophobic and van der Waals (VDW) interactions, although a few intermolecular H bonds exist in the binding interface (Figures 3B–3E; Table 2). Residues in helices A and C of IL-7 contact residues in the six loop regions connecting the β sheets of the IL-7Rα FNIII domains (Figures 3C and 3D). On average, apolar

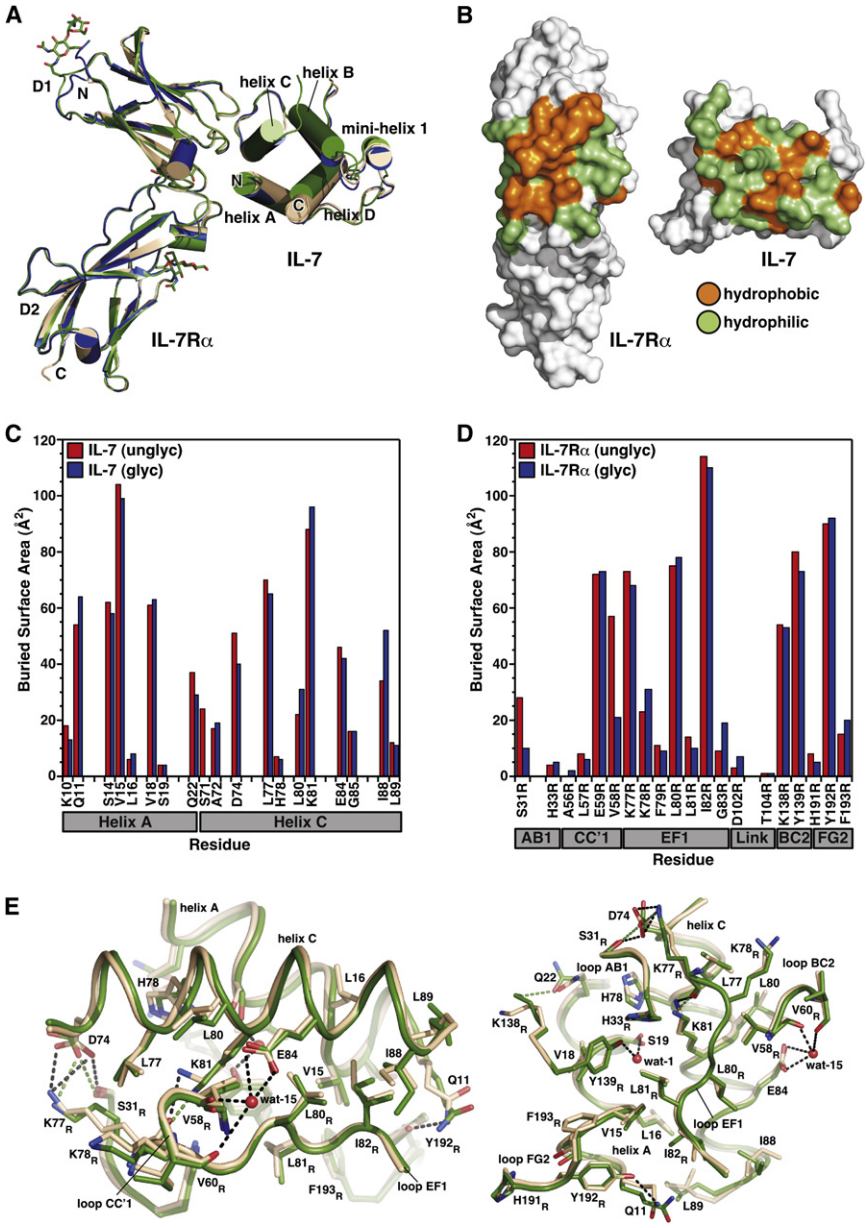

Figure 3. Structural Comparison between Unglycosylated and Glycosylated IL-7/IL-7Rα Complexes

(A) Superimposition of the unglycosylated structures (wheat and blue) onto the glycosylated structure (green) using the D1 and D2 domains of the receptors.

(B) Molecular surface view of IL-7 and IL-7Rα highlighting the hydrophobic (orange) and hydrophilic (lime green) residues in the binding interface.

(C and D) Bar graphs showing the amount of buried surface area for IL-7 (C) and IL-7Rα (D) in the unglycosylated (red bars) and glycosylated (blue bars) complexes. Secondary structure locations are labeled below the residues.

(E) Two views of the intermolecular interactions observed between the IL-7/IL-7Rα unglycosylated (wheat) and glycosylated (green) structures. H bonds are depicted as dashes colored black and green for the unglycosylated and glycosylated complexes, respectively.

residues dominate the contact interfaces for the IL-7/IL-7Rα structures over polar residues (47% versus 33%; Table 3). The two unglycosylated complexes in the asymmetric unit bury 735 and 720 Å^2 of surface area, whereas the glycosylated complex buries 705 Å^2 of surface area (Table 3).

Glycosylation of IL-7Rα does not influence its interaction with IL-7 through direct contacts at the binding interface with IL-7 (Figure 2D). The glycans attached to N45$_R$ face away from IL-7 on the back side of the D1 domain of IL-7Rα. The glycans attached to N29$_R$ and N131$_R$ are 10 and 15 Å away from the closest IL-7 atom, respectively. Even though N162$_R$, N212$_R$, and N213$_R$ could not be visualized in the electron density, their potentially attached glycans are not near the interface either. Ongoing biophysical and structural studies of the free states of unglycosylated and glycosylated IL-7 and IL-7Rα will determine how glycosylation affects molecular recognition events of IL-7Rα with IL-7.

The IL-7/IL-7Rα interfaces in all three structures involve similar H bonds, except for a couple of bonds and water-mediated interactions. The binding interfaces of both complexes share four common H bonds involving D74 and K81 of IL-7, but each complex has additional H bonds absent from the other complex (Figure 3E; Table 2). In the glycosylated complex, Q22 Oε1 from helix A forms a long H bond with K138$_R$ Nζ (3.4 Å), whereas, in the unglycosylated complex, the Y192$_R$ Oη forms an H bond with Q11 Nε2 (3.2 Å). Only one of the unglycosylated complexes in the asymmetric unit has an interface containing water-mediated interactions. Of the six water-mediated interactions observed in the unglycosylated structure, two H bonds form between the hydroxyl side chains of S19 of helix A and Y139$_R$, and four H bonds form between the side chain of E84 of helix C and the backbone carbonyls of V58$_R$ and V60$_R$ in loop CC′1 of IL-7Rα (Figure 3E). The differences observed in the H bonds among the three structures involve rotameric changes of the side chains requiring minimal energetic costs going from one structure to another.

DISCUSSION

IL-7/IL-7Rα Binding Mechanism

IL-7/IL-7Rα displays a more complex binding mechanism in comparison to other IL/receptor interactions in the γ_c family. The binding kinetics of IL-7 with either unglycosylated or glycosylated IL-7Rα involve a two-step reaction where an encounter complex, (IL-7:IL-7Rα)*, is observed before reaching the final

Table 2. Potential Hydrogen Bonds in Unglycosylated and Glycosylated IL-7/IL-7Rα Complexes

Unglycosylated IL-7/IL-7Rα Complex 1		
IL-7	IL-7Rα	Distance (Å)
Asp74 Oδ1	Lys77 Nζ	3.4
Asp74 Oδ1	Ser31 Oγ	3.2
Asp74 Oδ2	Lys77 Nζ	3.1
Lys81 Nε	Lys77 O	3.1
Gln11 Nε2	Tyr192 Oη	3.1
Wat-1	Ser19 (IL-7) Oγ	2.7
Wat-1	Tyr139 (IL-7Rα) Oη	2.6
Wat-15	Glu84 (IL-7) Oε1	3.5
Wat-15	Glu84 (IL-7) Oε2	3.6
Wat-15	Val58 (IL-7Rα) O	2.6
Wat-15	Val60 (IL-7Rα) O	3.7
Unglycosylated IL-7/IL-7Rα Complex 2		
Asp74 Oδ1	Lys77 Nζ	3.4
Asp74 Oδ1	Ser31 Oγ	3.3
Asp74 Oδ2	Lys77 Nζ	3.1
Lys81 Nζ	Lys77 O	2.9
Gln11 Nε2	Tyr192 Oη	3.2
Glycosylated IL-7/IL-7Rα Complex		
IL-7	IL-7Rα	
Gln22 Oε1	Lys138 Nζ	3.4
Asp74 Oδ2	Ser31 Oγ	3.3
Asp74 Oδ2	Lys77 Nζ	2.9
Asp74 Oδ1	Lys77 Nζ	3.6
Lys81 Nζ	Lys77 O	2.7

Table 3. Summary of Binding Interfaces of γ_c Complexes

Complex	BSA (Å^2)[a]	H Bonds	S_c[b]	% Polar Residues	% Apolar Residues
Unglyco IL-7/IL-7Rα 1	735	5	0.68	29.7	51.5
Unglyco IL-7/IL-7Rα 2	720	5	0.69	33.1	47.2
Glyco IL7/IL-7Rα	705	5	0.65	36.3	42.5
IL-2/IL-2Rβ	1350	8	0.74	39.3	24.1
IL-4/IL-4 binary	835	15	0.74	39.7	30.8
IL-4/IL-4Rα ternary	778	14	0.70	46.0	22.2

Values were calculated from PISA, CCP4, and the protein/protein interaction server at http://www.bioinformatics.sussex.ac.uk/protorp/index.html.

[a] Average buried surface area of the cytokine and receptor at the interface.

[b] Shape complementarity of the interface.

complex state ($k_{-1} > k_2$; Equation 1). In contrast, the SPR binding kinetics of IL-2, -4, and -21 to their CRH I receptors were fit best to a single-step reaction with a single on- and off-rate constant (k_1, k_{-1}) (Liparoto et al., 2002; Shen et al., 1996; Zhang et al., 2003). An encounter complex of these complexes may exist, but not observable using current methods. The significance of the two-step binding reaction of the human IL-7/IL-7Rα interaction and the dramatic enhancement of the k_1 on rate of IL-7 to glycosylated IL-7Rα are open questions that future studies will explore. Of note, the interaction between mouse IL-7 and full-length mouse IL-7Rα on a cell surface also displayed biphasic binding kinetics (Park et al., 1990).

IL-7Rα SCID Mutations

The point mutations in IL-7Rα that have been identified in patients suffering from SCID map to residues outside the binding epitope with IL-7, but localize to residues in the hydrophobic cores of the FNIII domains, cysteines of disulfide bonds, or the WSXWS motif (Figure 4; reviewed in Giliani et al., 2005). Five SCID mutations identified in the IL-7Rα D1 domain include $G8_RR$, $S24_RR$, $L35_RR$, $C54_RY$, and $C98_RY$. The $G8_RR$ mutation could not be mapped onto the IL-7Rα structure because residue G8 was not visible in the electron density of any of the IL-7Rα structures. $Ser24_R$ Oγ forms a H bond to $L130_R$ O that will be absent from the $S24_RR$ SCID mutation. The loss of this H bond and the need to accommodate a large Arg side chain probably causes the $S24_RR$ mutation to destabilize the linker connecting the D1 and D2 domains. The $L35_RR$ SCID mutation presumably unfolds the FNIII domain by forcing a bulky, polar side chain into the hydrophobic core of the D1 domain. SCID mutations $C54_RY$ and $C98_RY$ each remove a disulfide bond from IL-7Rα, thereby disrupting the folding/stability of the D1 domain.

SCID mutations in the D2 domain localize to or near the WSXWS motif between $W197_R$ and $S201_R$. The Trps, $W197_R$ and $W200_R$, of the WSXWS motif participate in extensive π cation interactions with Trp ($W158_R$), Lys ($K184_R$), and arginine ($R186_R$ and $R150_R$) side chains. Two SCID mutations convert what would be residues $W197_R$ and $R186_R$ to stop codons, resulting in termination of mRNA. Three other SCID mutations in the WSXWS motif include $S198_RN$, $W200_RC$, and $S201_RI$. $S198_R$ and $S201_R$ rigidify the D2 domain by orienting the G2 and F2 β strands through several Ser side-chain to main-chain H bonds. The SCID mutations $S198_RN$ and $S201_RI$ lack these critical H bonds. In addition to disrupting the core of the π cation interactions, $W200_RC$ may interfere with proper disulfide bond formation. Finally, SCID mutations $L115_RR$, $P112_RH$, and $P112_RS$ probably destabilize the hydrophobic core of the D2 domain. Studies of related CRH I cytokine receptors (GHR and EpoR) reported the WSXWS motif as crucial to proper folding of the ectodomains, binding of ligands, and functions (Baumgartner et al., 1994; Hilton et al., 1996).

IL-7/IL-7Rα Structural Comparison to γ_c Members

The binding interface between IL-7 and IL-7Rα differs from the interfaces between other ILs and receptors in the γ_c family in size, polarity, and specificity. The average buried surface area of the IL-7/IL-7Rα interface is 720 Å^2, whereas the buried surface areas of the IL-4/IL-4Rα binary and ternary complexes and IL-2/IL-2Rβ interfaces are 835, 778, and 1350 Å^2, respectively (Hage et al., 1999; Laporte et al., 2008; Wang et al., 2005) (Table 3). The IL-7/IL-7Rα interface predominantly involves apolar residues (average 47% apolar, 33% polar), the IL-4/IL-4Rα interface polar residues (27% apolar, 43% polar) (Hage et al., 1999; Laporte et al., 2008), and the IL-2/IL-2Rβ interface both apolar and polar residues (24% apolar, 39% polar) (Wang et al., 2005) (Figure 5). The IL-7/IL-7Rα interface comprises 5 H bonds, whereas the IL-4/IL-4Rα and IL-2/IL-2Rβ interfaces comprise 15, 14, and 8 H bonds, respectively (Hage et al., 1999; Laporte et al., 2008;

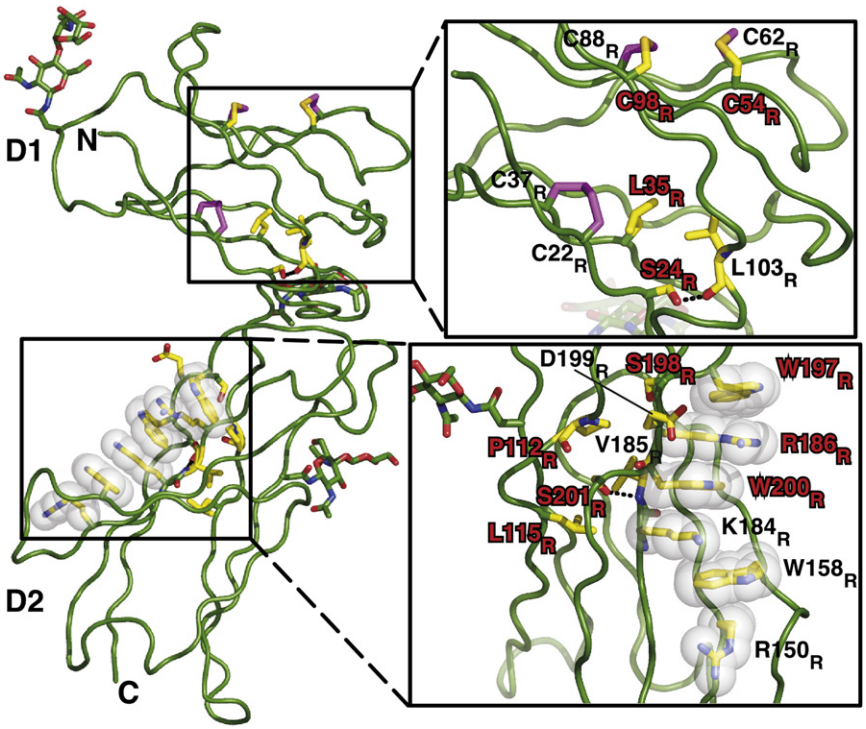

Figure 4. SCID Mutations Identified in Patients Are Mapped onto the Structure of the IL-7Rα Ectodomain

The WSXWS motif is depicted with yellow sticks and gray transparent CPK representations. H bonds between the backbone carbonyl of $L103_R$ with the $S24_R$ Oγ (2.7 Å) and $S201_R$ Oγ with $V185_R$ N (3.0 Å) are drawn as black dots. SCID residues are labeled in red.

Wang et al., 2005) (Table 3). Unlike the nonspecific hydrophobic and VDW contacts that dominate the IL-7/IL-7Rα interface, side-chain-specific hydrophilic contacts dominate the IL-4/IL-4Rα interface flanked by hydrophobic residues, whereas a mixture of hydrophobic and hydrophilic contacts comprise the interface of IL-2/IL-2Rβ (Hage et al., 1999; Wang et al., 2005). Moreover, the IL-7/IL-7Rα interface has the lowest shape complementarity value of 0.67 (average of three structures) compared with 0.74 and 0.72 (averaged) for the IL-2/IL-2Rβ and IL-4/IL-4Rα interfaces, respectively (Table 3). The IL-7/IL-7Rα interface is therefore the smallest, least polar, and least specific of the three interfaces.

The apolar, nonspecific nature of the IL-7/IL-7Rα interface and overall charge of IL-7 and IL-7Rα suggest that electrostatics influence the IL-7/IL-7Rα interaction less than the IL-4/IL-4Rα interaction but possibly more than the IL-2/IL-2Rβ interaction. Electrostatic attraction drives the IL-4/IL-4Rα interaction directly through charges in the interface and the overall charge of the molecules (Hage et al., 1999; Zhang et al., 2002b). The basic residues comprising the binding surface of positively charged IL-4 (pI 9.0) interact directly with the acidic and hydrophobic residues comprising the binding surface of negatively charged IL-4Rα (pI 5.1) (Figure 5B). Electrostatics play a less prominent role in the IL-2/IL-2Rβ interaction, because the overall charges of IL-2 (pI 7.1) and IL-2Rβ (pI 6.7) are neutral and the interface comprises both polar and apolar residues (Wang et al., 2005) (Figure 5C). A long-range electrostatic attraction may drive the interaction between IL-7 (pI 8.4) and IL-7Rα (pI 5.3) through complementary overall charges of the molecules. Even though apolar residues govern the IL-7/IL-7Rα interface, the IL-7 residues above and away from the interface are mainly basic, and the IL-7Rα residues distributed throughout the receptor except near the interface are mainly acidic (Figure 5A).

The orientation of the helices of the four-helix bundle of IL-7 varies from that of other γ_c ILs, possibly to present a distinct γ_c binding epitope. Backbone Cα superimpositions of the four-helix bundles (helices A–D) of IL-2 from the IL-2 quaternary complex (Wang et al., 2005), IL-4 from the binary and ternary complexes (Hage et al., 1999; Laporte et al., 2008), and IL-21 (Bondensgaard et al., 2007) onto IL-7 result in rmsds of 2.5 Å (60 Cα), 3.2 Å (62 Cα), 3.1 Å (62 Cα), and 2.4 Å (43 Cα), respectively (Figure S3). Similar backbone rmsds of each γ_c IL onto IL-7 were also obtained by superimposing only helices A and C or helices A, B, and C (Figure S3). The angular changes between helix D are smallest for IL-2 and IL-21 in comparison to IL-7 for the three different superimpositions by 7°–12° for IL-2 and 9°–12° for IL-21. The IL-4 binary and ternary complexes display larger helix D changes in comparison to IL-7, ranging from 14° to 26° depending on which helices were superimposed. These angular changes of the helices, particularly of helix D, presumably allow each IL to present a different binding surface for γ_c. The γ_c must differentiate among all of its different binding partners to carefully regulate signaling pathways. IL-7 possibly distinguishes itself within the four-helix bundle framework common to all γ_c ILs by not only varying the amino acid composition of helices A and D on its predicted γ_c binding surface but also by angular displacement of its helices.

Extending beyond the orientations of the four-helix bundle arrangements, the differences in the angular geometries between the FNIII D1 and D2 domains of IL-7Rα, IL-2Rβ, and IL-4Rα also suggest that either the IL-7/IL-7Rα complex, γ_c, or a combination of both structures must change conformation from the ones observed in both the IL-2 quaternary and IL-4 ternary complexes to form a productive IL-7/IL-7Rα/γ_c complex. Analysis was performed to determine FNIII domain geometries of the γ_c family members with the new IL-7Rα structures as described (Deivanayagam et al., 2000). Superimposition of either the D1 or D2 domains of IL-7Rα from both structures or the IL-4Rα structures (binary and ternary complexes) onto IL-2Rβ reveals that the elbow angle connecting the D1 and D2 domains varies slightly among the five structures (Figures 6A and 6B; Table S3). The changes of twist (τ) and swivel (σ) angles, however, show that the rotations relating the D1 and D2 domains of IL-7Rα are generally larger (D1 versus D2 superimpositions: $\Delta\tau = 14°, 21°$; $\Delta\sigma = 25°, 1°$) than IL-4Rα from the binary or ternary

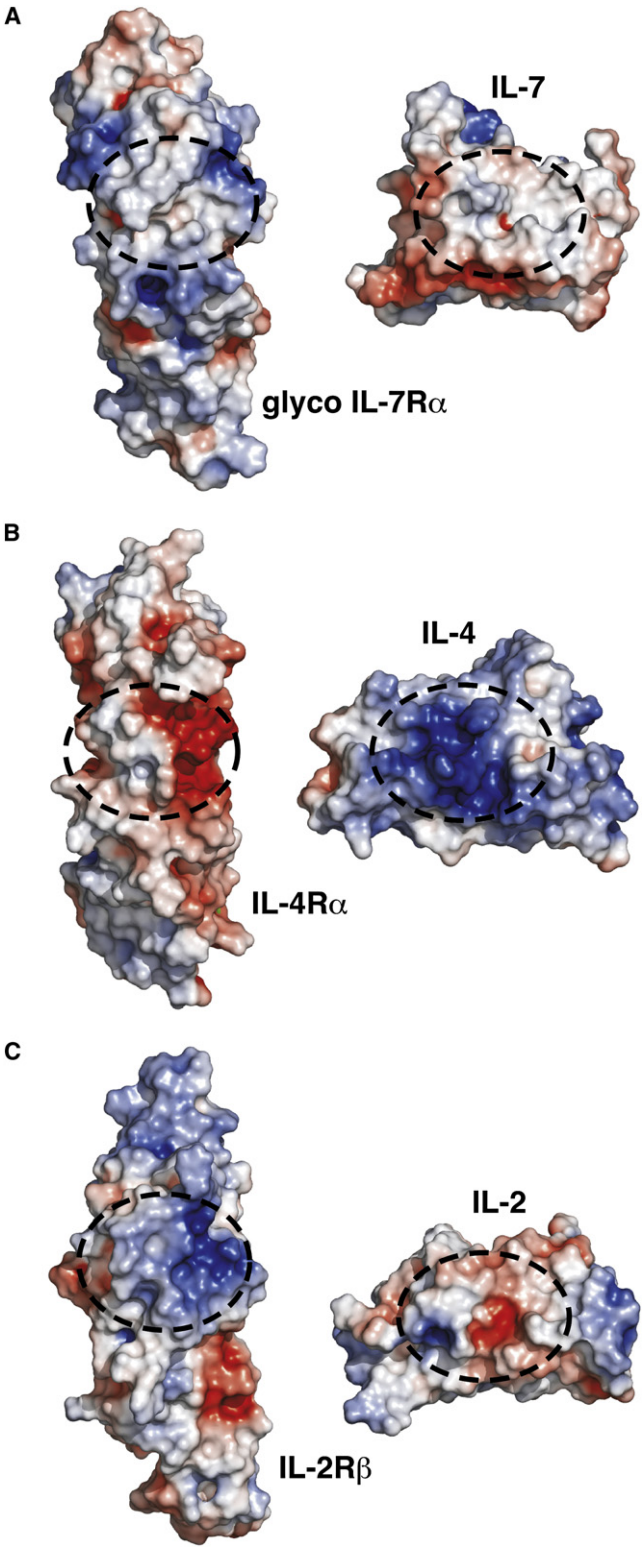

Figure 5. Electrostatic Surface Potentials of γ_c ILs and Receptors
(A) IL-7 and glycosylated IL-7Rα.
(B) IL-4 and IL-4Rα from Protein Data Bank (PDB) ID code 1IAR.
(C) IL-2 and IL-2Rβ from PDB ID code 2BFI. The electrostatic potential surfaces are displayed at a level of ±5 k_BT/e (blue, +; red, −). Contact areas between the interleukins and their receptors are marked by a dashed circle.

complexes (D1 versus D2 superimpositions: binary $\Delta\tau = 17°, 19°$; $\Delta\sigma = 10°, 9°$; ternary $\Delta\tau = 12°, 11°$; $\Delta\sigma = 9°, 1°$) in relation to IL-2Rβ. The considerable differences between the τ and σ angles relating the D1 and D2 domains of IL-7Rα with either IL-2Rβ or IL-4Rα prevent the unobstructed docking of the γ_c conformation from the IL-2 or IL-4 structures onto the IL-7/IL-7Rα structure. Superimposing the D1, D2, or both D1/D2 domains of the IL-7/IL-7Rα complex onto the corresponding domains of either the IL-2 quaternary or IL-4 ternary structures result in steric clashes between the D2 domains of IL-7Rα and γ_c, steric clashes between helix D and loop 1 of IL-7 with γ_c, or helices A/D of IL-7 being too far to contact γ_c (Figures 6C–6E; Figure S4). Thus, γ_c likely uses a different conformation from the one observed in either the IL-2 or IL-4 structures to productively form the IL-7/IL-7Rα/γ_c ternary complex.

Model of the IL-7/IL-7Rα/γ_c Complex

Data implicate a handful of residues on IL-7 and γ_c as important to productive formation of the IL-7/IL-7Rα/γ_c ternary complex (Olosz and Malek, 2002). Mutagenesis studies of IL-7 have yet to identify any residues important to the binding of γ_c; however, structural and mutagenesis data of other γ_c family members (Hage et al., 1999; Letzelter et al., 1998; Wang et al., 2005) consistently implicate helices A and D in the binding of γ_c. Analysis of the IL-7 structure in the IL-7/IL-7Rα complex reveals seven solvent-exposed residues on helix D that could interact with γ_c: R133, H136, E137, K139, T140, N143, and S144 (Figure 7). Mutagenesis studies of γ_c have identified three residues, Y103γ_c, G210γ_c, and N128γ_c, and the C160γ_c-C209γ_c disulfide bond, as crucial to the productive formation of the IL-7/IL-7Rα/γ_c complex (Olosz and Malek, 2002). Y103γ_c, G210γ_c, and the disulfide bond are also critical to the formation of complexes involving IL-2, -4, -15, and -21, whereas N128γ_c has been identified as important for complexes involving IL-7 and IL-21 (Olosz and Malek, 2002; Zhang et al., 2002a, 2003).

Using mutagenesis data (Olosz and Malek, 2002; Zhang et al., 2002a, 2003) and the IL-7/IL-7Rα and γ_c (Laporte et al., 2008; Wang et al., 2005) structures, we built a structure of the IL-7/IL-7Rα/γ_c complex to demonstrate the potential conformational change that γ_c must undergo to form an IL-7 ternary complex (Figure 7). The docking of γ_c was guided by bringing the Y103γ_c side chain, which packs in similar regions on both the IL-2 and IL-4 γ_c structures, within contact with K139 and T140 of IL-7. The model does not account for any interaction between helix A and the loop regions of γ_c, with the closest potential contact between the two being 5 Å. Also unlikely is the absence of interactions between the D2 domains of γ_c and IL-7Rα. The IL-2 and IL-4 γ_c structures revealed large binding interfaces between the D2 domains of γ_c with IL-2Rβ (1750 Å^2 surface area burial and 17 H bonds; Wang et al., 2005) and γ_c with IL-4Rα (1350 Å^2 surface area burial and 4 H bonds; Laporte et al., 2008). The closest contact between side chains of the D2 domains of γ_c and IL-7Rα is 7 Å (Figure 7). If the D2 domain interactions observed in both the IL-2 and IL-4 structures are conserved in the IL-7 complex, then γ_c must adopt a different conformation from the ones observed in the IL-2 and IL-4 structures (Laporte et al., 2008; Wang et al., 2005). A more acute elbow angle between the D1 and D2 domains of γ_c may allow interactions between helix A and the γ_c loops and between the D2

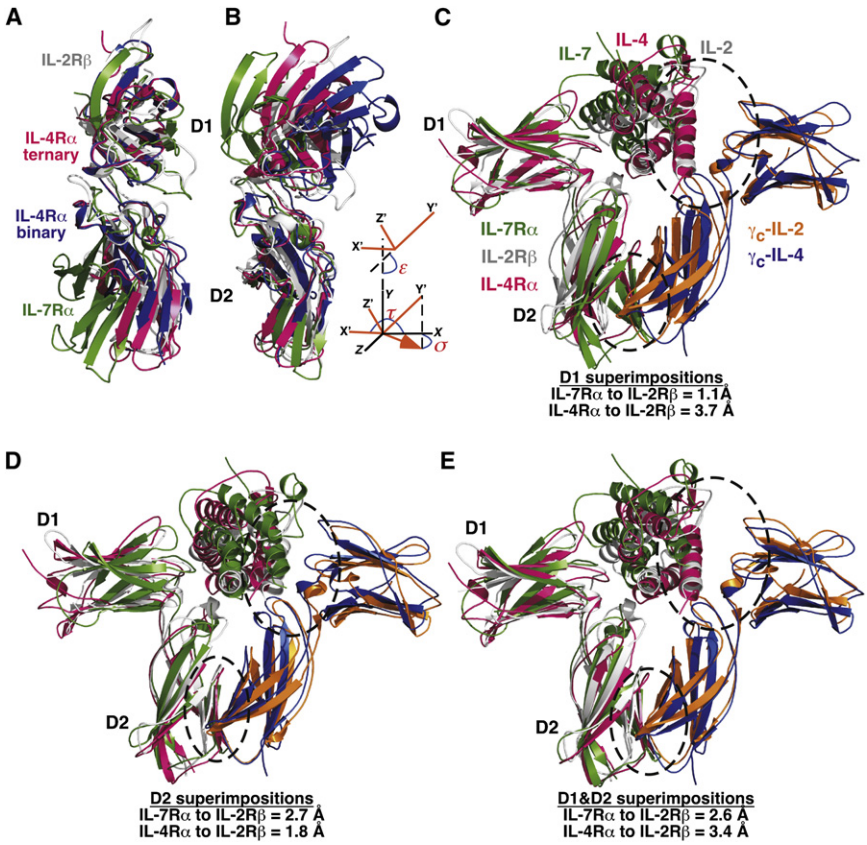

Figure 6. IL-7Rα Structural Comparison among the Known Receptor Structures of the γ_c Family

(A) Superimposition of the D1 domains of IL-7Rα (green, glycosylated structure), IL-4Rα from the binary complex (pink; PDB ID code 1IAR), and IL-4Rα from the ternary complex (magenta; PDB ID code 3BPL) individually superimposed onto the D1 domain of IL-2Rβ (gray; PDB ID code 2BFI).

(B) Superimposition of the D2 domains of the receptors as described in (A). The inset defines the three angles relating the two FNIII domains described previously (Deivanayagam et al., 2000). The elbow angle (ϵ) defines the angle between the two domains forming the distinctive L shape of the receptor. The twist angle (τ) represents the angle between the x axes of the D1 and D2 domains. The spin of the D2 domain in the x-z plane defines the swivel angle (σ).

(C) Superimpositions of the IL-7/IL-7Rα and IL-4 ternary complexes onto the IL-2 quaternary structures using only the D1 domains.

(D) Superimpositions of the IL-7/IL-7Rα and IL-4 ternary complexes onto the IL-2 quaternary structure using only the D2 domains.

(E) Superimpositions of the IL-7/IL-7Rα and IL-4 ternary complexes onto the IL-2 quaternary structures using both the D1 and D2 domains.

domains of IL-7Rα and γ_c. Crystal structure determination of the IL-7/IL-7Rα/γ_c complex is under way.

Structural-Functional Roles of IL-7Rα Glycosylation

Glycosylation of IL-7Rα could contribute to the interaction between IL-7 and IL-7Rα through at least two different mechanisms. First, glycosylation may be affecting the overall electrostatic potential of IL-7Rα. The global complementary charges of IL-7 (highly positive) and IL-7Rα (highly negative) may influence the binding of IL-7 and IL-7Rα, and glycosylation may, in turn, modulate those charges. For example, the negatively charged sialic acids increased the negative charge on erythropoietin (EPO) (dropping the pI from 9.2 to 4.6), thereby exacerbating the charge differential between EPO and its receptor *decreasing* the binding affinity by *only 12-fold* (*~9-fold slower on rate* between aglycosylated and glycosylated EPO), but increasing serum half-life (Darling et al., 2002). Yet, the degree of branching and the types of glycans typically determine to what extent glycosylation may affect the electrostatic potential, and the IL-7/IL-7Rα interaction was insensitive to variations in branching and glycans. Because glycosylated IL-7Rα binds IL-7 with the same affinity and k_1 on rate irrespective of branching and glycan type, and even with only the primary GlcNAc, glycosylation may affect the binding constants through a local rather than global electrostatic mechanism.

Second, glycosylation may also alter the conformations sampled by free IL-7Rα. Free IL-7Rα is likely undergoing conformational exchange between at least two states: nonbinding IL-7Rα and IL-7Rα poised to bind IL-7. The reason the binding kinetics fit best to a two-state exchange mechanism is likely that nonbinding IL-7Rα and IL-7Rα poised to bind IL-7 are in equilibrium with one another. Glycosylation may affect the frequency and duration with which free IL-7Rα visits these different conformations through electrostatics, sterics, overall stability, or a combination. By shifting the equilibrium toward the IL-7Rα conformation poised to bind IL-7, glycosylation of IL-7Rα may increase the binding k_1 on rate and affinity associated with the IL-7/IL-7Rα interaction.

Glycosylation could affect the conformational equilibrium of free IL-7Rα through changes local to the attached glycans or more globally. The differences between the unglycosylated and glycosylated IL-7Rα in complex with IL-7 are small overall, and the variations local to the glycans are subtle. All of the glycans extend away from the structure and do not make any contacts with residues besides their attached Asns, except a single H bond between the $N45_R$ glycan and residue $N47_R$. Because the IL-7/IL-7Rα interfaces of the unglycosylated and glycosylated structures superimpose with negligible rmsds, any changes induced locally by the glycans remain local and do not translate to changes at the interface. Globally, glycosylation may stabilize free IL-7Rα and the IL-7/IL-7Rα complex (free energy of unfolding, ΔG°_u). Thermodynamic studies of EPO showed that glycosylation increased ΔG°_u, thereby increasing the stability of the folded state (Darling et al., 2002; Egrie and Browne, 2001). In another example, studies have shown that the glycosylation of N297 of the C_H2 domain of the IgG-Fc arm leads to enhanced thermal unfolding relative to the unglycosylated form and that the glycans are essential for its binding/function to the Fc γ

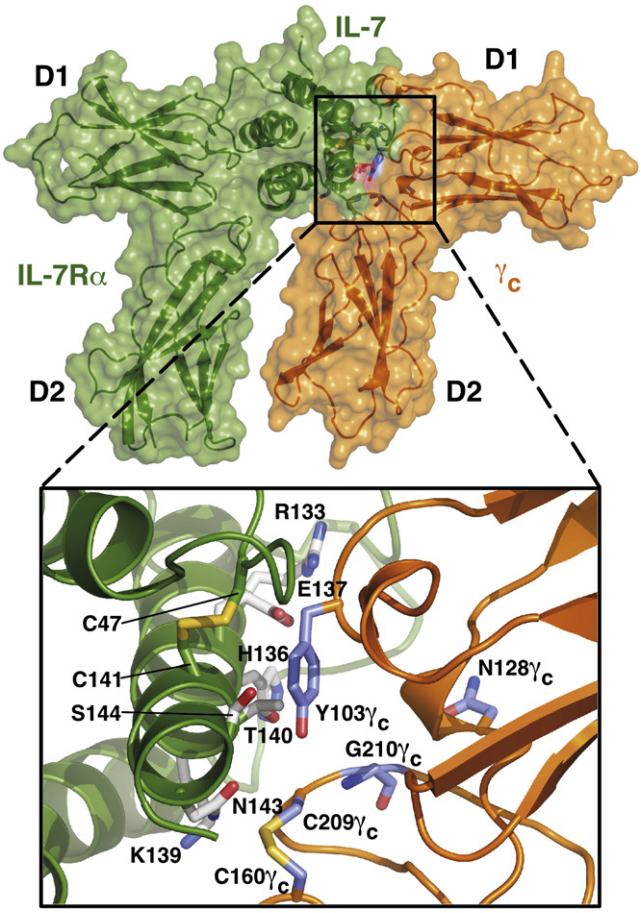

Figure 7. Hypothetical Model of the IL-7/IL-7Rα/γ_c Signaling Complex

Solvent-exposed IL-7 helix D residues are colored as white sticks. The γ_c (orange) residues shown to interact with the IL-7/IL-7Rα complex are colored purple.

receptor (FcγR) (Mimura et al., 2001), even though the N297 glycans (Fc fragment forms a dimer) do not participate directly in the binding interface of Fc:FcγR (Sondermann et al., 2000). Therefore, we posit that glycosylation increases the binding constants of the IL-7/IL-7Rα interaction by increasing the thermodynamic stability of IL-7Rα, the 1:1 complex, or a combination of both by shifting its conformational equilibrium to a state more conducive to binding IL-7.

EXPERIMENTAL PROCEDURES

Protein Expression and Purification

Proteins were expressed and purified from bacterial and S2 insect cells as described previously (Wickham and Walsh, 2007). Recombinant human IL-7Rα ectodomain from CHO cells was purchased from R&D Systems.

Endoglycosidase Treatment of IL-7Rα

Endoglycosidase reactions of IL-7Rα (S2) to trim the glycans directly from the Biacore sensor chips were performed as previously described (Logsdon et al., 2004) with the exception that 2500 U of Endo H was used. In addition, a reaction temperature of 37°C was used for both enzymes. Similar reactions were used using 1 μg of soluble E217C-IL-7Rα for the competition ELISAs.

SPR Analysis

Experiments were performed using a Biacore 2000 or 3000 SPR instrument. The IL-7Rα ectodomain coupling and binding kinetics were measured using a CM5 sensor chip at 25°C. IL-7Rα was coupled to a CM5 sensor chip using amine or thiol coupling. For thiol coupling using both *E. coli* (EC) and S2 (S2) insect expression systems, a C-terminal cysteine mutation (E217C) was engineered into the IL-7Rα ectodomain. To remove IL-7Rα intermolecular disulfide bonds, before thiol coupling, E217C-IL-7Rα was mildly reduced with 1.5 mM DTT for 30 min at 4°C. After reduction, IL-7Rα was immediately desalted (PD-10 column) into 10 mM $NaPO_4$ buffer (pH 7.4), concentrated to ~200 μl, and stored at 4°C.

In preparation for thiol coupling of IL-7Rα, the CM5 sensor chip was first washed with 10 mM HEPES (pH 7.4), 150 mM NaCl, 3 mM EDTA, and 0.005% Tween 20 at 10 μl/min for 10 min. Each flow cell was injected with 10 μl of N-hydroxysuccinimide/N-ethyl-N′-(3-dimethylaminopropyl)carbodiimide (NHS/EDC), followed by 20 μl of 2-(2-pyridinyldithio)ethaneamine hydrochloride (PDEA), and then 10–50 μl of reduced E217C-IL-7Rα (50–100 μg/ml in 10 mM sodium acetate [pH 4.5]) was injected over flow cells 2–4. Flow cell 1 served as a reference cell. Flow cells were blocked with a 35 μl injection of 50 mM reduced glutathione in 20 mM NaOAc (pH 4.5) with 1 M NaCl.

For amine coupling of IL-7Rα (CHO), the same procedure was performed as above, but the receptor was injected after the NHS/EDC activation step. Approximately 10–30 μl of IL-7Rα in PBS buffer was injected over flow cells 2–4 (50–100 μg/ml, typically 30 μl of IL-7Rα in 100 μl of 10 mM sodium acetate [pH 4.5]). Flow cell 1 served as a reference. Flow cells were blocked with a 35 μl injection of 1 M ethanolamine (pH 8.5).

Numerous SPR control experiments were performed for the binding interactions of IL-7 to both unglycosylated and glycosylated IL-7Rα that indicate that mass transport effects were negligible. Nonspecific binding was not observed when IL-7 was injected over the underivatized flow cells. SPR experiments measured at 50 μl/min involved 2-fold serial dilutions of five IL-7 concentrations determined by the binding affinity to the IL-7Rα ectodomain. Each 250 μl protein/buffer injection was followed by a 400 s dissociation period. The surface was regenerated for subsequent runs with a 5 μl injection of 4 M $MgCl_2$.

Sensorgrams were trimmed and double referenced (Morton et al., 1995) using BIAevaluation 4.1 before data analysis. The IL-7 binding interaction measured on either the thiol or amine IL-7Rα-coupled surfaces fit best to a two-step reaction model (Morton et al., 1995):

$$\text{IL-7} + \text{IL-7R}\alpha \underset{k_{-1}}{\overset{k_1}{\leftrightarrow}} (\text{IL-7:IL-7R}\alpha)^* \underset{k_{-2}}{\overset{k_2}{\leftrightarrow}} \text{IL-7:IL-7R}\alpha. \quad (1)$$

Apparent equilibrium dissociation constants (K_D) were calculated from

$$K_D = k_{-1}k_{-2}/k_1(k_2 + k_{-2}). \quad (2)$$

Sensorgrams were globally analyzed using ClampXP (Myszka and Morton, 1998), and the binding kinetic parameters were determined from at least three separate experiments.

Competition ELISA

Unlabeled IL-7 displaced horseradish peroxidase (HRP; Pierce) -conjugated IL-7 from immobilized IL-7Rα. Unglycosylated and glycosylated IL-7Rα variants with the E217C mutation were thiol coupled to biotin-HPDB (N-(6-[biotinamido]hexyl)-3′-(2′-pyridyldithio)-propionamide) (Pierce). Maxisorb 96-well plates were coated with 5 μg/ml of NeutrAvidin (Pierce) in 50 mM $NaHCO_3$ (pH 9) overnight at 4°C. The plates were washed four times with PBS and 0.05% Tween 20 (PBS-Tween). The 96-well plates were blocked with Superblock-PBS (Pierce) and 0.05% Tween 20 for 2 hr. The unglycosylated (6 nM) and glycosylated (1 nM) biotin-IL-7Rα variants were immobilized for 2 hr. The plates were washed four times with PBS-Tween. Concentrations of 250 and 3 nM HRP-IL-7 were used for the unglycosylated and glycosylated biotin-IL-7Rα displacements, respectively. Two-fold serial dilutions of unlabeled IL-7 were initiated at 100 and 3.2 μM for the immobilized unglycosylated and glycosylated receptors, respectively, and mixed with the fixed HRP-IL-7 concentrations. The plates were incubated for 2 hr and washed eight times with PBS-Tween. The plates were developed using HRP chemistry and measured at 450 nm. Displacement curves were fit to a single-site competition model and experiments were triplicated.

Crystallization, Data Collection, and Structure Determination

Protein crystallization of the unglycosylated and glycosylated complexes has been reported elsewhere (Wickham and Walsh, 2007). The protein complexes that diffracted incorporated a surface-loop mutation, E106A, in IL-7 (Wickham and Walsh, 2007). Another glycosylated native data set was collected on a larger pyramidal shaped crystal and merged with a previously described data set (Wickham and Walsh, 2007). In addition, a platinum derivative of the glycosylated complex was prepared by soaking a crystal in 10 mM K_2PtCl_6 for 2 hr. Protein crystals were flash frozen in liquid nitrogen after transfer into 15%–20% glycerol with the appropriate mother liquor. X-ray data were collected at the Structural Biology Center 19ID beamline, Advanced Photon Source, Argonne National Laboratories, Chicago, IL, USA and processed using HKL-3000 (Minor et al., 2006).

The crystal structure of the unglycosylated complex was solved using a three-wavelength multiwavelength anomalous diffraction data set collected on a crystal that incorporated selenomethionine into E106A-IL-7 (EC). Mass spectrometry indicated that 5–6 selenomethionines were substituted for the 6 methionines in E106A-IL-7. SHELXD (Schneider and Sheldrick, 2002) only located 5 of the 10–12 predicted SeMet heavy atoms from the SeMet-substituted complex crystal. Heavy-atom refinement, phasing, and density modification were performed using autoSHARP to 3.0 Å (Bricogne et al., 2003; Vonrhein et al., 2007). Automatic chain tracing, noncrystallographic symmetry (NCS) averaging, and phase combination of the model and experimental information were performed using RESOLVE (Terwilliger, 2003), DM (Cowtan and Main, 1998), and SIGMAA (CCP, 1994). Coot (Emsley and Cowtan, 2004) was used for model building. Simulated annealing torsional angle dynamics, conjugate gradient energy minimization, an overall anisotropic temperature factor and bulk solvent correction, and B factor refinement were performed using CNS 1.2 (Brunger, 2007). NCS restraints were employed using a force constant of 150 kcal/mol $Å^2$ as listed in Table S1 by comparing the R_{free} values with and without the restraints.

The crystal structure of the glycosylated IL-7 (EC):IL-7Rα (S2) complex was solved by combining phases of a Pt derivative with a molecular replacement solution from EPMR (Kissinger et al., 2001) using the unglycosylated IL-7/IL-7Rα complex as the search model. Two Pt sites were identified by SHELXD. Experimental phases were calculated in autoSHARP using the single isomorphous with anomalous scatter (SIRAS) strategy. The phase-combined electron density map was sharper with the Pt data. Molprobity (Davis et al., 2007), CCP4 (CCP, 1994), and PISA (Krissinel and Henrick, 2007) were used for structural validation and analysis. All structural figures were created using PyMOL (http://pymol.sourceforge.net).

ACCESSION NUMBERS

Atomic coordinates and structure factors have been deposited in the Protein Data Bank under ID codes 3DI2 and 3DI3 for the unglycosylated and glycosylated complexes, respectively.

SUPPLEMENTAL DATA

Supplemental Data include four figures and three tables and can be found with this article online at http://www.cell.com/structure/supplemental/S0969-2126(08)00431-0.

ACKNOWLEDGMENTS

S.T.R.W. dedicates this manuscript to Joshua Wand, William DeGrado, and Anthony Kossiakoff. We thank Apostolos Gittis for crystallography advice. We thank Naomi Logsdon and Mark Walter for help with S2 insect cells. We thank Mike Carson for the program to calculate receptor domain angles. X-ray data were collected used the Structural Biology Center 19ID beamline at the APS at Argonne National Laboratory, under contract DE-AC02-06CH11357. We thank the SBC staff for their assistance. C.A.M. was supported by a postdoctoral fellowship from the American Heart Association (725595B). This research was supported by funds from the College of Medicine and Ohio Board of Regents and grants from the AHA (535131N) and NIH (AI72142) to S.T.R.W.

Received: July 23, 2008
Revised: October 16, 2008
Accepted: October 22, 2008
Published: January 13, 2009

REFERENCES

Aoki, K., Perlman, M., Lim, J.M., Cantu, R., Wells, L., and Tiemeyer, M. (2007). Dynamic developmental elaboration of N-linked glycan complexity in the *Drosophila melanogaster* embryo. J. Biol. Chem. *282*, 9127–9142.

Baumgartner, J.W., Wells, C.A., Chen, C.M., and Waters, M.J. (1994). The role of the WSXWS equivalent motif in growth hormone receptor function. J. Biol. Chem. *269*, 29094–29101.

Bondensgaard, K., Breinholt, J., Madsen, D., Omkvist, D.H., Kang, L., Worsaae, A., Becker, P., Schiodt, C.B., and Hjorth, S.A. (2007). The existence of multiple conformers of interleukin-21 directs engineering of a superpotent analogue. J. Biol. Chem. *282*, 23326–23336.

Bricogne, G., Vonrhein, C., Flensburg, C., Schiltz, M., and Paciorek, W. (2003). Generation, representation and flow of phase information in structure determination: recent developments in and around SHARP 2.0. Acta Crystallogr. D Biol. Crystallogr. *59*, 2023–2030.

Brunger, A.T. (2007). Version 1.2 of the Crystallography and NMR system. Nat. Protoc. *2*, 2728–2733.

CCP4 (Collaborative Computational Project, Number 4). (1994). The CCP4 suite: programs for protein crystallography. Acta Crystallogr. D Biol. Crystallogr. *50*, 760–763.

Cosenza, L., Sweeney, E., and Murphy, J.R. (1997). Disulfide bond assignment in human interleukin-7 by matrix-assisted laser desorption/ionization mass spectroscopy and site-directed cysteine to serine mutational analysis. J. Biol. Chem. *272*, 32995–33000.

Cosenza, L., Rosenbach, A., White, J.V., Murphy, J.R., and Smith, T. (2000). Comparative model building of interleukin-7 using interleukin-4 as a template: a structural hypothesis that displays atypical surface chemistry in helix D important for receptor activation. Protein Sci. *9*, 916–926.

Cowtan, K., and Main, P. (1998). Miscellaneous algorithms for density modification. Acta Crystallogr. D Biol. Crystallogr. *54*, 487–493.

Darling, R.J., Kuchibhotla, U., Glaesner, W., Micanovic, R., Witcher, D.R., and Beals, J.M. (2002). Glycosylation of erythropoietin affects receptor binding kinetics: role of electrostatic interactions. Biochemistry *41*, 14524–14531.

Davis, I.W., Leaver-Fay, A., Chen, V.B., Block, J.N., Kapral, G.J., Wang, X., Murray, L.W., Arendall, W.B., III, Snoeyink, J., Richardson, J.S., and Richardson, D.C. (2007). MolProbity: all-atom contacts and structure validation for proteins and nucleic acids. Nucleic Acids Res. *35*, W375–W383.

Deivanayagam, C.C., Rich, R.L., Carson, M., Owens, R.T., Danthuluri, S., Bice, T., Hook, M., and Narayana, S.V. (2000). Novel fold and assembly of the repetitive B region of the *Staphylococcus aureus* collagen-binding surface protein. Structure *8*, 67–78.

Egrie, J.C., and Browne, J.K. (2001). Development and characterization of novel erythropoiesis stimulating protein (NESP). Br. J. Cancer *84* (*Suppl 1*), 3–10.

Emsley, P., and Cowtan, K. (2004). Coot: model-building tools for molecular graphics. Acta Crystallogr. D Biol. Crystallogr. *60*, 2126–2132.

Giliani, S., Mori, L., de Saint Basile, G., Le Deist, F., Rodriguez-Perez, C., Forino, C., Mazzolari, E., Dupuis, S., Elhasid, R., Kessel, A., et al. (2005). Interleukin-7 receptor α (IL-7Rα) deficiency: cellular and molecular bases. Analysis of clinical, immunological, and molecular features in 16 novel patients. Immunol. Rev. *203*, 110–126.

Goodwin, R.G., Lupton, S., Schmierer, A., Hjerrild, K.J., Jerzy, R., Clevenger, W., Gillis, S., Cosman, D., and Namen, A.E. (1989). Human interleukin 7: molecular cloning and growth factor activity on human and murine B-lineage cells. Proc. Natl. Acad. Sci. USA *86*, 302–306.

Hage, T., Sebald, W., and Reinemer, P. (1999). Crystal structure of the interleukin-4/receptor α chain complex reveals a mosaic binding interface. Cell *97*, 271–281.

Hilton, D.J., Watowich, S.S., Katz, L., and Lodish, H.F. (1996). Saturation mutagenesis of the WSXWS motif of the erythropoietin receptor. J. Biol. Chem. *271*, 4699–4708.

Kissinger, C.R., Gehlhaar, D.K., Smith, B.A., and Bouzida, D. (2001). Molecular replacement by evolutionary search. Acta Crystallogr. D Biol. Crystallogr. *57*, 1474–1479.

Krissinel, E., and Henrick, K. (2007). Inference of macromolecular assemblies from crystalline state. J. Mol. Biol. *372*, 774–797.

Laporte, S.L., Juo, Z.S., Vaclavikova, J., Colf, L.A., Qi, X., Heller, N.M., Keegan, A.D., and Garcia, K.C. (2008). Molecular and structural basis of cytokine receptor pleiotropy in the interleukin-4/13 system. Cell *132*, 259–272.

Leonard, W.J. (2002). TSLP: finally in the limelight. Nat. Immunol. *3*, 605–607.

Letzelter, F., Wang, Y., and Sebald, W. (1998). The interleukin-4 site-2 epitope determining binding of the common receptor γ chain. Eur. J. Biochem. *257*, 11–20.

Liparoto, S.F., Myszka, D.G., Wu, Z., Goldstein, B., Laue, T.M., and Ciardelli, T.L. (2002). Analysis of the role of the interleukin-2 receptor γ chain in ligand binding. Biochemistry *41*, 2543–2551.

Logsdon, N.J., Jones, B.C., Allman, J.C., Izotova, L., Schwartz, B., Pestka, S., and Walter, M.R. (2004). The IL-10R2 binding hot spot on IL-22 is located on the N-terminal helix and is dependent on N-linked glycosylation. J. Mol. Biol. *342*, 503–514.

Matsumoto, M., Misawa, S., Tsumoto, K., Kumagai, I., Hayashi, H., and Kobayashi, Y. (2003). On-column refolding and characterization of soluble human interleukin-15 receptor α-chain produced in *Escherichia coli*. Protein Expr. Purif. *31*, 64–71.

Mazzucchelli, R., and Durum, S.K. (2007). Interleukin-7 receptor expression: intelligent design. Nat. Rev. Immunol. *7*, 144–154.

Mimura, Y., Sondermann, P., Ghirlando, R., Lund, J., Young, S.P., Goodall, M., and Jefferis, R. (2001). Role of oligosaccharide residues of IgG1-Fc in Fc γ RIIb binding. J. Biol. Chem. *276*, 45539–45547.

Minor, W., Cymborowski, M., Otwinowski, Z., and Chruszcz, M. (2006). HKL-3000: the integration of data reduction and structure solution—from diffraction images to an initial model in minutes. Acta Crystallogr. D Biol. Crystallogr. *62*, 859–866.

Morton, T.A., Myszka, D.G., and Chaiken, I.M. (1995). Interpreting complex binding kinetics from optical biosensors: a comparison of analysis by linearization, the integrated rate equation, and numerical integration. Anal. Biochem. *227*, 176–185.

Myszka, D.G., and Morton, T.A. (1998). CLAMP: a biosensor kinetic data analysis program. Trends Biochem. Sci. *23*, 149–150.

Olosz, F., and Malek, T.R. (2002). Structural basis for binding multiple ligands by the common cytokine receptor γ-chain. J. Biol. Chem. *277*, 12047–12052.

Park, L.S., Friend, D.J., Schmierer, A.E., Dower, S.K., and Namen, A.E. (1990). Murine interleukin 7 (IL-7) receptor. Characterization on an IL-7-dependent cell line. J. Exp. Med. *171*, 1073–1089.

Puel, A., Ziegler, S.F., Buckley, R.H., and Leonard, W.J. (1998). Defective IL7R expression in T(−)B(+)NK(+) severe combined immunodeficiency. Nat. Genet. *20*, 394–397.

Rickert, M., Boulanger, M.J., Goriatcheva, N., and Garcia, K.C. (2004). Compensatory energetic mechanisms mediating the assembly of signaling complexes between interleukin-2 and its α, β, and γ (c) receptors. J. Mol. Biol. *339*, 1115–1128.

Schneider, T.R., and Sheldrick, G.M. (2002). Substructure solution with SHELXD. Acta Crystallogr. D Biol. Crystallogr. *58*, 1772–1779.

Shen, B.J., Hage, T., and Sebald, W. (1996). Global and local determinants for the kinetics of interleukin-4/interleukin-4 receptor α chain interaction. A biosensor study employing recombinant interleukin-4-binding protein. Eur. J. Biochem. *240*, 252–261.

Sondermann, P., Huber, R., Oosthuizen, V., and Jacob, U. (2000). The 3.2-Å crystal structure of the human IgG1 Fc fragment-Fc γRIII complex. Nature *406*, 267–273.

Sportes, C., and Gress, R.E. (2007). Interleukin-7 immunotherapy. Adv. Exp. Med. Biol. *601*, 321–333.

Terwilliger, T.C. (2003). SOLVE and RESOLVE: automated structure solution and density modification. Methods Enzymol. *374*, 22–37.

vanderSpek, J.C., Sutherland, J.A., Gill, B.M., Gorgun, G., Foss, F.M., and Murphy, J.R. (2002). Structure function analysis of interleukin 7: requirement for an aromatic ring at position 143 of helix D. Cytokine *17*, 227–233.

Vonrhein, C., Blanc, E., Roversi, P., and Bricogne, G. (2007). Automated structure solution with autoSHARP. Methods Mol. Biol. *364*, 215–230.

Wang, X., Rickert, M., and Garcia, K.C. (2005). Structure of the quaternary complex of interleukin-2 with its α, β, and γ_c receptors. Science *310*, 1159–1163.

Wickham, J., Jr., and Walsh, S.T. (2007). Crystallization and preliminary X-ray diffraction of human interleukin-7 bound to unglycosylated and glycosylated forms of its α receptor. Acta Crystallogr. Sect. F Struct. Biol. Cryst. Commun. *63*, 865–869.

Yoon, S.I., Logsdon, N.J., Sheikh, F., Donnelly, R.P., and Walter, M.R. (2006). Conformational changes mediate interleukin-10 receptor 2 (IL-10R2) binding to IL-10 and assembly of the signaling complex. J. Biol. Chem. *281*, 35088–35096.

Zhang, J.L., Buehner, M., and Sebald, W. (2002a). Functional epitope of common γ chain for interleukin-4 binding. Eur. J. Biochem. *269*, 1490–1499.

Zhang, J.L., Simeonowa, I., Wang, Y., and Sebald, W. (2002b). The high-affinity interaction of human IL-4 and the receptor α chain is constituted by two independent binding clusters. J. Mol. Biol. *315*, 399–407.

Zhang, J.L., Foster, D., and Sebald, W. (2003). Human IL-21 and IL-4 bind to partially overlapping epitopes of common γ-chain. Biochem. Biophys. Res. Commun. *300*, 291–296.